NJC

Accepted Manuscript

This is an *Accepted Manuscript*, which has been through the Royal Society of Chemistry peer review process and has been accepted for publication.

Accepted Manuscripts are published online shortly after acceptance, before technical editing, formatting and proof reading. Using this free service, authors can make their results available to the community, in citable form, before we publish the edited article. We will replace this *Accepted Manuscript* with the edited and formatted *Advance Article* as soon as it is available.

You can find more information about *Accepted Manuscripts* in the Information for Authors.

Please note that technical editing may introduce minor changes to the text and/or graphics, which may alter content. The journal's standard Terms & Conditions and the Ethical guidelines still apply. In no event shall the Royal Society of Chemistry be held responsible for any errors or omissions in this *Accepted Manuscript* or any consequences arising from the use of any information it contains.

ROYAL SOCIETY OF CHEMISTRY

www.rsc.org/njc

Novel hierarchically dispersed mesoporous silica spheres: Effective adsorbents for mercury from wastewater and its thermodynamic study

Seenu Ravi, [a] Manickam Selvaraj, *[a] Hyun Park, [b] Ho-Hwan Chun, [b] and Chang-Sik Ha [c]

[a] *School of Chemical and Biomolecular Engineering, Pusan National University, Busan 609-735, Korea.*

[b] *Global Core Research Centre for Ships and Offshore Plants, Pusan National University, Busan 609 735, Korea.*

[c] *Department of Polymer Science and Engineering, Pusan National University, Busan 609-735, Korea.*

***** *Corresponding Author*
E-mail: chems@pnu.edu.
Tel.: +82 51 510 2397
Fax: +82 51 512 8563

Abstract

Novel hierarchically dispersed spherical mesoporous silica (HSMS) was synthesized using a surfactant mixture of fluorocarbon (FC-4), cetyl-trimethyl ammonium bromide (CTAB), and block copolymer Pluronic F127 (PF127). This material was functionalized with thiol groups by a direct one-pot method (T-HSMS). The obtained HSMS and T-HSMS possess a cubic morphology with $lm\bar{3}m$ space group and a particle diameter of 75–200 nm. The HSMS and T-HSMS materials exhibit large free surface areas exceeding 844 and 663 m^2/g and their pore radii of approximately 3.2 and 3.1 nm, respectively. The synthesized materials were characterized using small angle X-ray scattering, N_2-physisorption studies, scanning electron microscopy, transmission electron microscopy, and Fourier transform infrared spectroscopy studies. The efficacy of mercury adsorption by T-HSMS was studied at different temperatures such as 283, 298, and 313 K. The obtained results were fitted with Langmuir adsorption isothermal plot. The changes in negative Gibbs free energy values for the spontaneity process were calculated. Mercury could be successfully desorbed using thiourea in a 2-M HCl solution, and the adsorbents could be subsequently reused without severe loss of their activity in repeated adsorption tests.

Key words: Surfactant mixtures, IBN-1, Fluorocarbon surfactant, Dispersed silica, Mercury adsorption

1. Introduction

Anthropogenic mercury rises in water is being a serious threat to the biosystem owing to its persistence, volatility, and bioaccumulation. The presence of mercury in aquatic environments commonly endangers resident organisms and human health via seafood consumption. An aerobic action of microorganism on to the mercury compounds are accused for the bioaccumulation process [1]. General anthropogenic sources of inorganic mercury are fossil-fuel combustion, mining, and cement production [2]. Ingenious prevention of seawater and drinking water sources from mercury contaminated waste can reduce the occurrence of poisonous methyl mercury. The currently employed approaches for the removal of toxic pollutants from wastewater are adsorption techniques including reverse osmosis, ion exchange and coagulation processes [3-7]. Among these, the adsorption process is considered to be simple and economical. Sulfur-based hybrid mesoporous silica [8,9], mesoporous carbon[10], magnetic porous nanoparticles [11-15], and granular activated carbon [16,17] have shown tremendous capability in the removal of hazardous mercury ions. The focus has been on developing efficient and eco-friendly adsorbents to avoid causing further environmental toxicity.

Since, mesoporous silica materials are eco-friendly, recent research has been focused on synthesis of mesoporous silica materials with their prominent textural properties which includes excellent surface area, particle size, and pore size; these properties have attracted worldwide interest for the applications such as heavy-metal adsorption [18-22], controlled drug delivery [23-25], chemical-sensor development [26], and catalysis [27-30]. Such advantageous textural properties are pivotal for adsorbents to possess appropriate adsorption capacities for the specific

species. Selective functionalization and choice of nanoparticle morphology can influence the adsorption process of specific metal ions [31]. Mesoporous silica nano particles (MSNs) with particle sizes of less than 500 nm have been widely employed in various pharmaceutical applications such as in the development of drugs and biosensors and in the identification of genes and proteins [32-36]. MSNs with cubic $lm\bar{3}m$ space group have an interesting pore arrangement, which can provide a highly opened pore host that affords easy access for metal guest species. In the course of new material synthesis, co-surfactants have crucial role to transit the geometrical nature of MSNs. Recently, J.Y. Ying et al. synthesized orderly cubic $lm\bar{3}m$ mesoporous silica using Pluronic PF127 and fluorocarbon surfactant (FC-4) [37]. Similarly, Huo et al. synthesized cubic SBA-1 using HTEABr and PAA surfactants [38]. Moreover, some of the mesoporous materials have been synthesized by using three surfactants, for example Chengxiang Shi et al. synthesized hierarchically mesoporous silica single-crystalline nanorods with a three-dimensional cubic $Fm\bar{3}m$ mesostructure using CTAB, p123, and PAA surfactants [39].

Tae-wan Kim et al. reported the facile synthesis of monodispersed spherical MCM-48 particles with la3d mesopore geometry using a PF127 and CTAB surfactant mixture [40] and the synthesis of ordered irregular surface IBN-1 mesoporous silica encouraged us to prepare hierarchically dispersed spherical mesoporous silica (modified IBN-1) is as shown in scheme 1. The chemistry of demixing and reorganization effect of fluorocarbon surfactants with nonionic surfactants can change the physicochemical properties of the resulting nano silica particles [41, 42]. However, no one has so far reported the synthesis of mesoporous silica using these three surfactants and they are, CTAB, PF127 and FC-4. In contrast, an ample number of reports exist on the adsorption of heavy metals by thiol-functionalized mesoporous silica; nanosorbents are also emerging as the most commonly used type of sorbents for heavy-metal sorption from aqueous

media.

In the present work, we synthesized hierarchically cubic $lm\bar{3}m$ space group mesoporous silica by a solvothermal method. The HSMS mesoporous silica nanoparticles with controllable pore geometry were fabricated using the surfactant mixture CTAB/PF127/FC-4. In addition, we studied the effect of thiol-functionalization of HSMS and its mercury adsorption behavior as a function of various parameters such as pH, temperature, and time. Moreover, thermodynamic parameters were studied with respect to the temperatures.

2. Results and discussion

2.1 Synthesis and structural characterization of the HSMS and thiol functionalized HSMS

Hierarchically dispersed spherical mesoporous silica (HSMS) was synthesized using a mixture of three different surfactants: PF127, CTAB, and FC-4. Triblock copolymer Pluronic PF127 was used as the principal template, followed by CTAB, and the fluorocarbon were used as the secondary templates in the synthesis medium. CTAB and PF127 coassemble to form complex colloids by electrostatic interactions between the hydrophobic and hydrophilic terminals [40]. The fluorocarbon surfactant FC-4 was also infused into the complex. To this complex suspension, the silica precursor TEOS was added to coassemble with the complex templates to form silica-based mesoporous materials. To examine the adsorption nature of this new mesoporous material, it was functionalized with 3-mercaptotrimethoxysilane (3-MPS) by a direct method. Since thiol groups shows selective interactions with mercury, they can be exploited for a sustainable adsorption process [18].

The SAXS pattern of the calcined sample exhibited three different peaks, which were indexed to (110), (200), and (211) characteristic diffraction patterns of a cubic symmetry arrangement (Figure 1). This obtained lattice pattern and a d-spacing of 10.1 nm confirm that the HSMS material possesses $lm\bar{3}m$ symmetry with interconnected spherical pores. The unit cell parameters determined for the HSMS and T-HSMS particles are summarized in Table 1.

The morphology of HSMS was observed from the SEM and TEM images are shown in Figure 2. The SEM images of the HSMS and T-HSMS particles in Figure 2a and 2b shows that they possess a spherical morphology with a particle diameter ranging between 75 to 200 nm and this spherical particle size range is explained by the mole ratios of CTAB/PF127/FC-4 surfactant molecules. This hierarchical spherical geometry was attributed to the miscibility nature of CTAB with nonionic P127 surfactants as revealed from the formation of monodispersed spherical MCM-48 mesoporous silica with $la\bar{3}d$ mesostructure [40] and also CTAB can act as an emulsion formation agent to obtain regular mesoporous silica when used in combination with nonionic surfactants [39]. These statements were suggesting that in the synthesis of HSMS particle the packing parameters of CTAB and PF127 micelle were influenced by the addition of fluorocarbon surfactant and are ultimately changes the nature of micelle formation from $la\bar{3}d$ to $lm\bar{3}m$; at the same time the existence of CTAB surfactants organizes the micelle to ordered spherical in nature. Upon adding the silica precursor (TEOS) to the colloidal suspension of the PF127/CTAB/FC-4 complex an ordered hierarchical particle sizes as well as the pore sizes with $lm\bar{3}m$ pore arrangement were formed. The obtained monodispersed particles in TEM image Figure 2c illustrated that they possess spherical particles of interconnected pore system with small pore sizes. Similarly, the TEM image in Figure 2d shows that the particle size remains almost the

same even after functionalization with 3-MPS.

Nitrogen physisorption experiments were performed to study the textural properties of the calcined HSMS and extracted T-HSMS materials. The nitrogen adsorption isothermal plots of the HSMS and T-HSMS materials showed type IV isotherms with H2 hysteresis loops (Figure 3) [42-43]. These observations were associated with the capillary condensation in cubic mesopores; at relative pressures P/P_0 of 0.4–0.7, large, porous mesostructures with specific BET surface areas of 844 and 663 m^2/g were obtained for the HSMS and T-HSMS materials, respectively. The surface area of HSMS was quite higher than the reported IBN-1 mesoporous silicas. T-HSMS differs in the desorption branch where the convergence of the adsorption and desorption branches is downshifted to P/P_0 ~0.35, in comparison with ~0.4 for HSMS; this deviation of the hysteresis loop is attributed to the reduction in the pore volumes. Simultaneously, decrease in pore diameter value was observed upon the addition of 3-MPS (Table 1).

The functionalization was confirmed from the FT-IR spectra of the HSMS and T-HSMS materials (Figure 4). The propyl groups attached to the silicon framework were confirmed by the $–CH_2–$ stretching bands at 2930 cm^{-1}, confirming the attachment of organic moieties onto the silica surface; the band at 1451 cm^{-1} was assigned to the $–CH_2–$ symmetric bending mode vibration. A large broad band between 3600 and 3200 cm^{-1} was observed, which was attributed to the O–H stretching mode of the silanol groups. The absorption bands at 1084 and 800 cm^{-1} were assigned to Si–O–Si and Si–O stretching vibrations, respectively, and the bands at 961 cm^{-1} were characteristic of Si–OH stretching vibrations [44]. The extent of bonding nature of silicon environment in the HSMS was also confirmed by 29Silicon CP/MAS NMR spectroscopy is

displayed in figure 5. There were three distinct peaks at the range of -92, -101 and -110 attributing siloxane binding environment of silicon without hydroxyl groups [$(SiO)_4$—Si], isolated silanol groups [$(SiO)_3$—Si(OH)], and germinal silanol groups [$(SiO)_2$—$Si(OH)_2$] which are denoted as Q^2, Q^3 and Q^4 respectively [45]. Moreover the quantitative amount of sulphur in the T-HSMS material was calculated using Elemental analysis and summarized in the table 1.

The synthesis method of monodispersed MCM-48 and IBN-1 mesoporous silicas are explained that nonionic PF127 inclined to mix with different surfactants to produce ordered mesoporous materials. Hence we have achieved the synthesis of regular monodispersed cubic $lm\bar{3}m$ mesoporous silica (modified IBN-1 or HSMS), templated by the mixture of three different surfactants CTAB with PF127 and FC-4. Since cubic mesoporous silica gives easy access to the guest species, T-HSMS might be useful in the mercury adsorption process.

2.2 Adsorption studies

2.2.1 Effect of pH and time

The effect of pH on the adsorption of Hg^{2+} onto HSMS was tested in the pH range 2–10 for 50 ppm mercury solution. The optimum pH for the maximum removal of Hg^{2+} was found at pH 5 (Figure 6a). The rate of adsorption was varying with respect to pH values as a consequence of hydrating effect of metal ions when in contact with aqueous solution. The effective sizes of hydrated species of metal ions in aqueous solution is depending on the charges of the species, i.e., Hg^{2+} > $Hg(OH)^+$ > $Hg(OH)_2$. The mobility of charged hydrated species with smaller effective size is higher in comparison with larger hydrated Hg^{2+} species thus resulting in

increased adsorption rate during adsorbate/adsorbent interaction with increase in pH value [47, 48].

The adsorption of Hg^{2+} on T-HSMS at various initial concentrations (10–100 mg L^{-1}) was carried out over different periods of time (10–3600 min) at optimum pH 5. The degree of adsorption is faster at the initial stages due to the availability of free sites and it becomes slower in the later stage. The mercury-removal efficiency by T-HSMS at an initial concentration of 50 mg/L was calculated at regular time intervals as shown in Figure 6b.

2.2.2 Adsorption isotherms

The equilibrium adsorption isotherm is one measure to understand the mechanism of adsorption systems. For performing adsorption studies, mixtures of the synthesized T-HSMS materials with aqueous solutions containing known amounts of Hg^{2+} were prepared. The mixtures were stirred until equilibrium was reached. The adsorption isotherms of Hg^{2+} at 10, 25, and 40 °C are shown in Figure 7a.

There is an increase in the equilibrium adsorption capacity with the increasing initial concentration of Hg^{2+}. Langmuir isothermal model is widely used to investigate isothermal data. These isotherms not only explain the adsorption capacity but also give an insight into the surface properties and adsorbent/adsorbate affinity constants [49,50]. The Langmuir isotherm model assumes that adsorption takes place at specific homogeneous sites within the adsorbent by monolayer adsorption without any interaction between the adsorbed molecules. The Langmuir adsorption isotherm is established by the following relation:

$$q_e = \frac{q_m b C_e}{1 + b C_e}$$

This above equation can also be linearly written as

$$\frac{C_e}{q_e} = \frac{1}{b q_m} + \frac{C_e}{q_m}$$

where C_e is the equilibrium concentration of adsorbate entities in the solution (mmol L^{-1}), q_e defines the amount of adsorbate entities adsorbed per unit amount of the adsorbent at equilibrium (mmol g^{-1}), q_m represents the maximum adsorption capacity of the adsorbent (mmol g^{-1}), and b is defined as the affinity of the binding sites or the Langmuir constant (L $mmol^{-1}$). The Hg^{2+} adsorption isotherm of T-HSMS exhibits typical Langmuir behavior, similar to other thiol-functionalized mesoporous materials [51], suggesting monolayer adsorption at independent binding sites.

Adsorption kinetics data, the Langmuir isotherm models were shown in Figure 7b. From the Langmuir isotherm models, the maximum mercury binding capacity determined for HSMS is 0.367 mmol/g, and the calculated Langmuir constant (b) and correlation coefficient factors (R^2) are summarized in Table 2. In addition for the Langmuir adsorption isotherm, the calculated R^2 values are 0.9974, 0.9836, and 0.9830 at 283, 298, and 313 K, respectively. The obtained datas revealed that adsorption capacity of T-HSMS was higher than several other organo modified mesoporous silicas and silica gels [52-55].

2.2.3 Adsorption thermodynamics

The adsorption thermodynamics describe the changes in the Gibbs energy (G), enthalpy (H), and

entropy (S) during the adsorption process. These parameters are helpful to understand the adsorption feasibility and mechanism. The following classical equations are employed to study the adsorption thermodynamics:

$$\Delta G^o = -RT \ln K$$

Where K is the distribution constant, ΔH° and ΔS° can be calculated from the slope and intercept of the Van't Hoff's plot of ln K vs 1/T as shown in figure 8.

$$\ln K_c = \frac{\Delta S^o}{2.303R} - \frac{\Delta H^o}{2.303RT}$$

where R is the gas constant (R = 8.314 J/K/mol) and T is the temperature (K). The Van't Hoff plot of ln K against 1/T furnished the change in the entropy and changes in the enthalpy of the adsorption process, as summarized in Table 3. The negative ΔG° values confirm that the adsorption of Hg^{2+} on T-HSMS was a spontaneous process at all studied temperatures, and the decreasing values of ΔG° from -1.529 to -3.252 kJ/mol indicates the increasing adsorption tendency of T-HSMS. The positive values of ΔH° (+14.65 kJ/mol/K) shows that the adsorption process is endothermic, as an increase in the adsorption capacity of the particles was observed with an increase in the temperature, whereas the positive value of ΔS° (+57.03 J/K/mol) represents the increasing randomness at the adsorbent surface during the adsorption, which ultimately leads to an increase in the adsorption efficiency.

3. Conclusion

We have successfully synthesized hierarchically dispersed spherical mesoporous silica with a

well-ordered cubic $lm\bar{3}m$ mesostructure by choosing mixture of three different surfactants such as CTAB, PF127 and fluorocarbon FC-4. The porosity of HSMS was maintained about 3 nm by judiciously choosing the mole ratio of above three templates. Hence we concluded that it is easy to control the pore size of IBN-1 type mesoporous silica by typically choosing the mole ratios of the above given templates which also explains the possibilities of geometrical transition state from $la\bar{3}d$ MCM-48 monodispersed silica to $lm\bar{3}m$ cubic mesoporous silica (IBN-1type). The functionalization on HSMS mesoporous silica does not affect their hierarchy while it does on IBN-1 mesoporous silica. In addition the mercury adsorption behavior of thiol functionalized HSMS was investigated as a function of different parameters such as pH, temperature, and time. The material was found to be promising in the way, it can adsorb ~99%; even at lower mercury concentrations. Subsequently thermodynamic studies were done and ensure the adsorption of mercury is spontaneous with negative Gibbs free energy values.

4. Experiments

4.1 Material synthesis

A typical synthesis of HSMS was performed by judiciously choosing the mole ratios of CTAB/PF127/FC-4/TEOS/HCl and H_2O are 0.082/0.0023/0.072/1/0.062 and 192 respectively. CTAB, PF127, and FC-4 were dissolved in acidified water under magnetic stirring at 30 °C until a clear solution formed. Subsequently, tetraethylorthosilicate (TEOS) was added drop wise into the synthetic solution, and the reaction was stirred for 24–36 h at 30 °C. The reaction mixture was then transferred into a Teflon-lined autoclave and heated to 100 °C for the next 24–36 h. Finally, the mixture was filtered, and the shiny as-synthesized mesoporous material was dried

and calcined in a muffle furnace at 550 °C for 6 h; the resultant material was denoted as HSMS. Using the same procedure, 3-mercaptotrimethoxysilane (3-MPS) 0.1 mole was incorporated into the mesoporous material by a cocondensation method. The resultant as-synthesized material was stirred at reflux in ethanol:HCl (99:1) for 12 h. The material was then filtered and dried in an oven at 60 °C and denoted as T-HSMS.

4.2 Characterization

Small angle X-ray scattering (SAXS) was performed at the Pohang Accelerator Laboratory (PAL) (POSTECH, South Korea) with Co-Kα radiation (λ = 1.608 Å) in the energy range 4–16 keV (energy resolution: $\Delta E/E = 5 \times 10^{-4}$; photon flux: 10^{10}–10^{11} ph./s, beam size: <1 mm^2) over the scan range 0.4 $nm^{-1} < q < 4.0\ nm^{-1}$. Scanning electron microscopy (SEM) images were recorded on a JEOL JSM-6700F instrument. Transmission electron microscopy (TEM) images were recorded on a JEOL 2010 electron microscope operating at 200 kV. The powder samples were dispersed in ethanol and then deposited and dried on a perforated Cu grid. The images were recorded at magnifications of 150,000× and 200,000×. Nitrogen adsorption and desorption isotherms were measured using an ASAP 2020 surface area and pore size analyzer. Prior to the measurements, the samples were dehydrated at 95 °C for 5 h. The BET (Brunauer–Emmett–Teller) method was used to calculate the specific surface area. The pore size distribution was calculated from the analysis of the isotherm desorption branch by the BJH (Barret–Joyner–Halenda) method coupled with the apparatus software. The infrared spectra were recorded on a Nicolet 6700 FT-IR spectrometer. ^{29}Si CP/MAS NMR measurement was carried out on a Bruker ADVANCE II+ 400 MHz NMR system. Magic angle spinning was performed at 6 kHz spinning rate and the contact time was fixed at 2 ms in the experiment.

4.3 Mercury-uptake studies

The adsorption of mercury (II) cations by T-HSMS was investigated in a 50-mL glass vial. First, 25 mg of the T-HSMS was mixed with 25 mL of a stock solution of metal ions (10–120 ppm). The adsorption process was conducted at 25, 30, and 40 °C on an orbital shaker at a shaking speed of 150 rpm. The adsorptions were examined at different concentrations of Hg^{2+}. The equilibrium constant (q_e) was determined using the following equation:

$$q_e = (C_i - C_e) \times (V / M)$$

where C_i is the initial concentration, C_e is the equilibrium concentration, V is the volume of the solution, and M is the mass of the adsorbent. The concentration of metal ions remaining in the solution after the adsorption process as a function of different parameters such as time, pH, and temperature was analyzed. After 24 h, samples were removed, filtered through a 0.2–μm filter, and analyzed for mercury content. The Hg^{2+} quantity was determined using Direct Mercury Analyzer (DMA–80, Milestone).

4.4 Adsorbent regeneration

Recycling and regenerating the adsorbent plays a significant part in sorption studies for practical applications. Typically, 0.1 g of mercury-loaded T-HSMS adsorbent was treated with acidified thiourea (3 M HCl + 2% thiourea solution) and stirred for 6 h at room temperature, and then the treated adsorbent sample was thoroughly washed with ethanol, water, and dried at 60 °C for 12 h. The first regenerated 0.1g adsorbent was treated into 50 ppm mercury solution and the adsorption showed ~96% removal of mercury in the 2nd cycle. The materials were then regenerated using the same procedure and used over repeated cycles. Interestingly, 87% was

removed in the third cycle. The removal efficiency is slightly reduced in subsequent cycles; however, it was still above 75% in the fourth cycle, as shown in Figure 9, is displaying the promising adsorption behavior of T-HSMS materials.

Acknowledgment

This research work was supported by Basic Science Research Program through the National Research Foundation (NRF) of Korea (2012-0007172), BK21 PLUS through NRF (21A20131800002), and Korea government (MSIP) through GCRC-SOP (2011-0030013).

References

1 T.W. Clarkson, *J. Trace Elem. Exp. Med*., 1998, **11,** 303.

2 X.L. Jin, C. Yu and Y.F. Li, *J. Hazard. Mater*., 2011, **186,** 1672.

3 K. Linde and A.S. Jonsson, *Desalination*, 1995, **103,** 223.

4 M. rahni and B. Legube, *Water research*, 1996**, 30,** 1149.

5 A. Oehmen, D. Vergel, J. Fradinho, M.A.M. Reis, J.G. Crespo and S. Velizarov, *J. Hazard. Mater*., 2014, **264**, 65.

6 S. Oha, T. Kang and H. Kim, *Journal of Membrane Science*, 2007, **301,** 118.

7 G.H. Zhao and Y.F. Li, *J. Hazard. Mater*., 2010, **175**, 715.

8 H.Y. Wu, C.H. Liao, Y.C. Pan, C.L. Yeh and H.M. Kao, *Microporous Mesoporous Mater*., 2009, **119**, 109.

9 E.D. Canck, L. Lapeire, J.D. Clercq, F. Verpoort and P.V.D. Voort, *Langmuir*, 2010, **26**, 10076.

10 Y. Shin, G.E. Fryxell, W. Um, K. Parker, S.V. Mattigod and R. Skaggs, *Adv. Funct.*

Mater., 2007, **17**, 2897.

11 A. Sinha and N.R. Jana, *Chem. Commun*., 2012, **48**, 9272.

12 F. He, W. Wang, J. Moon, J. Howe, E. M. Pierce and L. Liang, *ACS Appl. Mater. Interfaces*, 2012, **4**, 4373.

13 X. Chen, K.F. Lam, Q. Zhang, B. Pan, M. Arruebo and K.L. Yeung, *J. Phys. Chem. C*, 2009, **113,** 9804.

14 J. Liu and X. Du, *J. Mater. Chem*., 2011, **21**, 6981.

15 K. Cheng, Y.M. Zhou, Z.Y. Sun, H.B. Hu, H. Zhong, X.K. Konga and Q.W. Chen, *Dalton Trans*., 2012, **41**, 5854.

16 H.C. Hsi, M.J. Rood, M.Rostam-Abadi, S. Chen and R. Chang, *Environ. Sci. Technol*., 2001, **35**, 2785.

17 W. Liu, R.D. Vidic and T.D. Brown, Environ. Sci. Technol., 2000, **34**, 483.

18 S. Ravi and M. Selvaraj*, Dalton Trans*., 2014, **43**, 5299.

19 A.M. Liu, K. Hidajat, S. Kawi and D.Y. Zhao, *Chem. Commun*., 2000, 1145.

20 P. J. Chiu, S. Vetrivel, A. S. T. Chiang and H. M. Kao, *New J. Chem*., 2011, **35**, 489.

21 J. Liuab and X. Du, *J. Mater. Chem*., 2011, **21**, 6981.

22 S.A. Idris, C.M. Davidson, C. McManamon, and M.A. Morris*, J. Hazard. Mater*., 2011, **185**, 898.

23 N. Mal, M. Fujiwara and Y. Tanaka, *Nature*, 2003, **421**, 350.

24 Y. Chen, H. Chen, M. Ma, F. Chen, L. Guo, L. Zhang and J. Shi, *J. Mater. Chem*., 2011, **21**, 5290.

25 P. Yang, S. Gai and J. Lin, *Chem. Soc. Rev*., 2012, **41**, 3679.

26 P. Van Der Voort, C. Vercaemst, D. Schaubroeck and F. Verpoort, *Phys. Chem.*

Chem. Phys. 2008, **10**, 347.

27 I.K. Mbaraka, D.R. Radu, V.S.-Y. Lin and B.H. Shanks, *Journal of Catalysis*, 2003. **219**, 329.

28 C. Jiang, K. Hara and A. Fukuoka, *Angew. Chem. Int. Ed*., 2013, **52**, 6265.

29 M. Selvaraj and S. Kawi, *Microporous mesoporous mater*. 2008, **109**, 458.

30 C.M.A. Parlett, K. Wilson and A.F. Lee*, Chem. Soc. Rev*., 2013, **42**, 3876.

31 B.G. Trewyn, S. Giri, I.I. Slowing and V.S.Y. Lin, *Chem. Commun*., 2007, 3236.

32 S. Angelos, M. Liong, E. Choi and J. I. Zink*, Chem. Eng. J*., 2008, **137**, 4.

33 D.R. Radu, C.Y. Lai, K. Jeftinija, E.W. Rowe, S. Jeftinija and V.S.Y. Lin, *J. Am. Chem. Soc*., 2004, **126**, 13216.

34 B.G. Trewyn, C.M. Whitman and V.S.Y. Lin, *Nano Lett*., 2004, **4**, 2139.

35 I. Slowing, B.G. Trewyn and V.S.-Y. Lin, *J. Am. Chem. Soc*., 2006, **128**, 14792.

36 M. Vallet-Regí, F. Balas and D. Arcos, *Angew. Chem. Int. Ed*., 2007, **46**, 7548.

37 Y. Han and J.Y. Ying, Angew. *Chem. int. Ed*., 2005, **44**, 288.

38 Q. Huo, D. I. Margolese, U. Ciesla, P. Feng, T. E. Gier, P. Sieger, R. Leon, P. M. Petroff, F. Schuth and G. D. Stucky, Nature, 1994, **368**, 317.

39 C. Shi, S. Deng, J. Wang, P. Sun and T. Chen, *J. Mater. Chem. A* 2013, **1**, 14555.

40 T.W. Kim, P.W. Chung and V.S.-Y. Lin, *Chem. Mater*., 2010, **22**, 5093.

41 R. Xing, H.J. Lehmler, B.L. Knutson and S.E. Rankin, *Langmuir,* 2009, **25**, 6486.

42 D. Li, Y. Han, J. Song, L. Zhao, X. Xu, Y. Di and F.S. xiao, *Chem. Eur. J*., 2004, **10**, 5911.

43 K.Sing, D. Everett, R. Haul, L. Moscou, R. Pierotti, J. Rouquerol, and T. Siemieniewska, *Pure Appl. Chem*. 1985, **57**, 603.

44 R. Atchudan, A. Pandurangan and J. Joo, *Microporous Mesoporous Mater*., 2013, **175**, 161.

45 P. T. Tanev and T. J. Pinnavaia, *Chem. Mater*., 1996, **8,** 2068.

46 D. Zhao, Q. Huo, J. Feng, B. F. Chmelka and G. D. Stucky, *J. Am. Chem. Soc*., 1998, **120**, 6024.

47 G. Li, Z. Zhao, J. Liu and G. Jiang, *J. Hazard. Mater*., 2011, **192**, 277.

48 C. Delacote, F. O. M. Gaslain, B. Lebeau and A. Walcarius, *Talanta* 2009, **79**, 877.

49 J.L. Vivero-Escoto, M. Carboni, C.W. Abney, K.E. deKrafft and W. Lin, *Microporous Mesoporous Mater*., 2013, **180**, 22.

50 O. Hakami, Y. Zhang and C.J. Banks*, Water Res*., 2012, **46**, 3913.

51 J. Aguado, J.M. Arsuaga and A. Arencibia*, Ind. Eng. Chem. Res*., 2005, **44**, 3665–3671.

52 E. De Canck, L. Lapeire, J. De Clercq, F. Verpoort and P. Van Der Voort, *Langmuir*, 2010, **26**, 10076–10083.

53 A.R. Cestari, E.F.S. Vieira, E.C.N. Lopes and R.G. da Silva, *Journal of Colloid and Interface Science,* 2004, **272**, 271–276.

54 D. Perez-Quintanilla, I. del Hierro, M. Fajardo and I. Sierra, *Microporous Mesoporous Mater*., 2006, **89**, 58–68.

55 A. Khan, F. Mahmood, M.Y. Khokhar and S. Ahmed, *React. Funct. Polym*., 2006, **66**, 1014–1020.

Figures

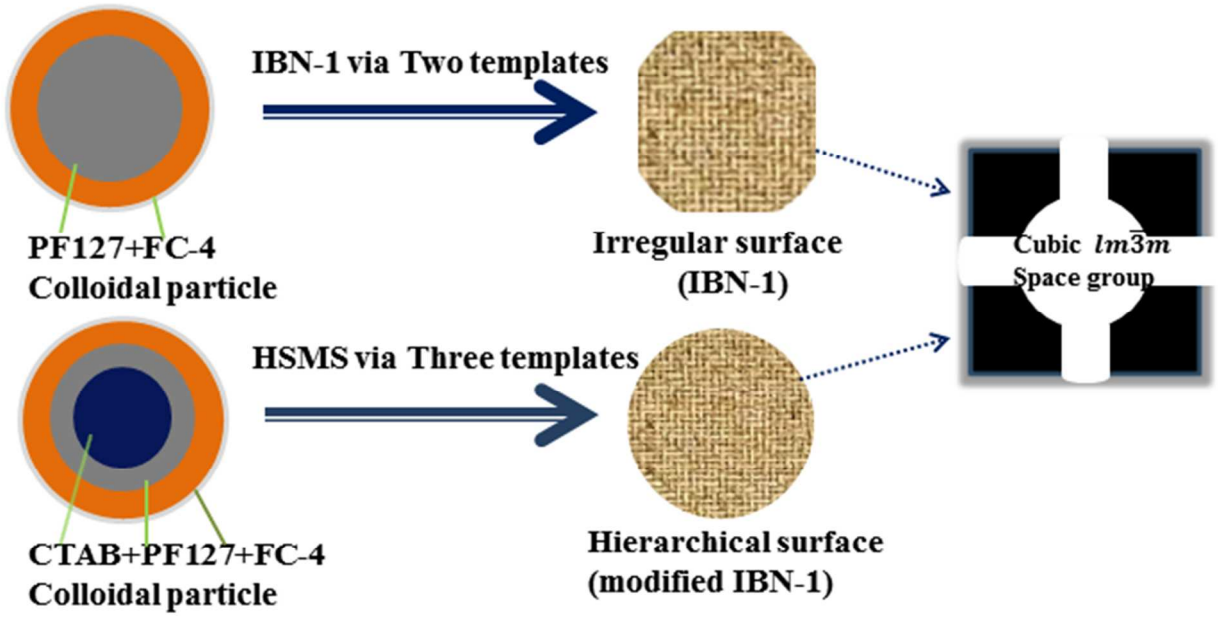

Scheme 1: Schematic representation for HSMS (modified IBN-1) formation.

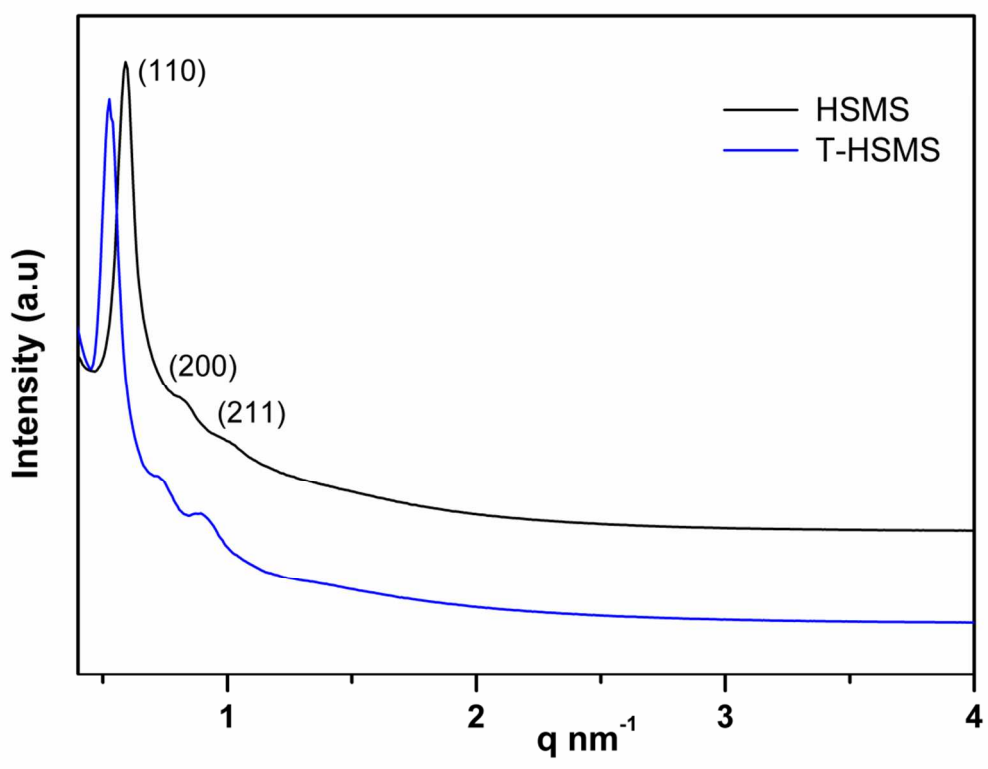

Figure 1: The SAXS patterns of HSMS and T-HSMS

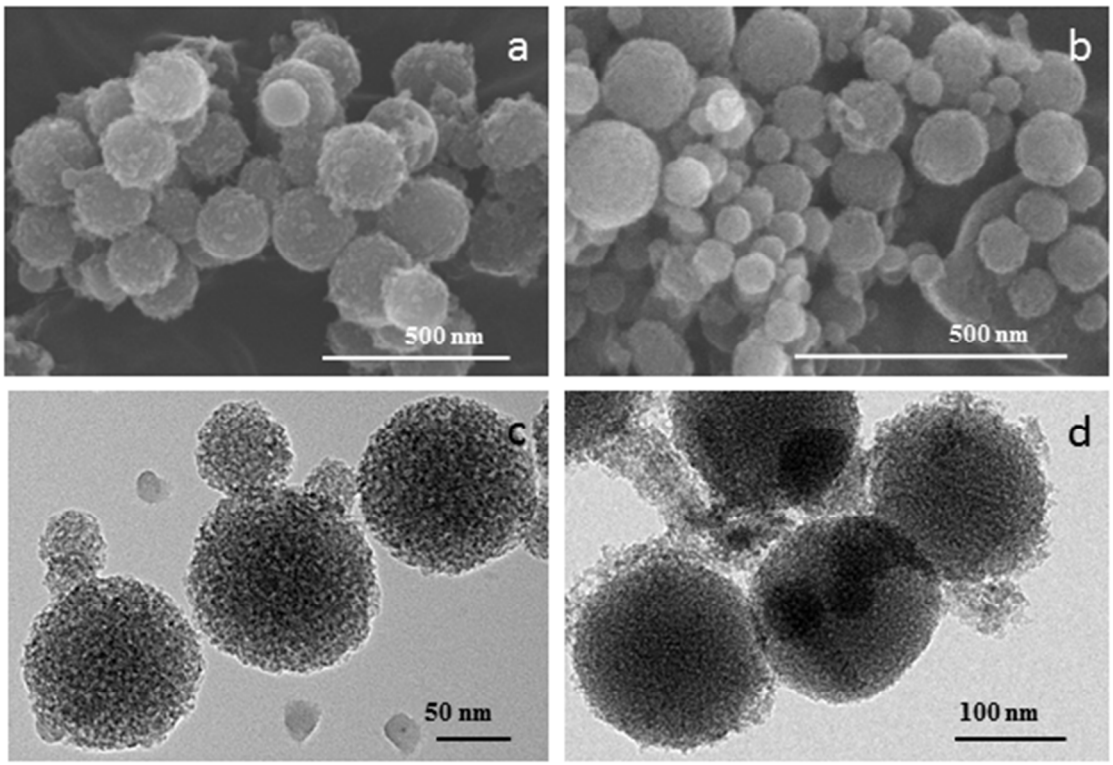

Figure 2: The SEM and TEM images of HSMS (a & c) and T-HSMS (b & d).

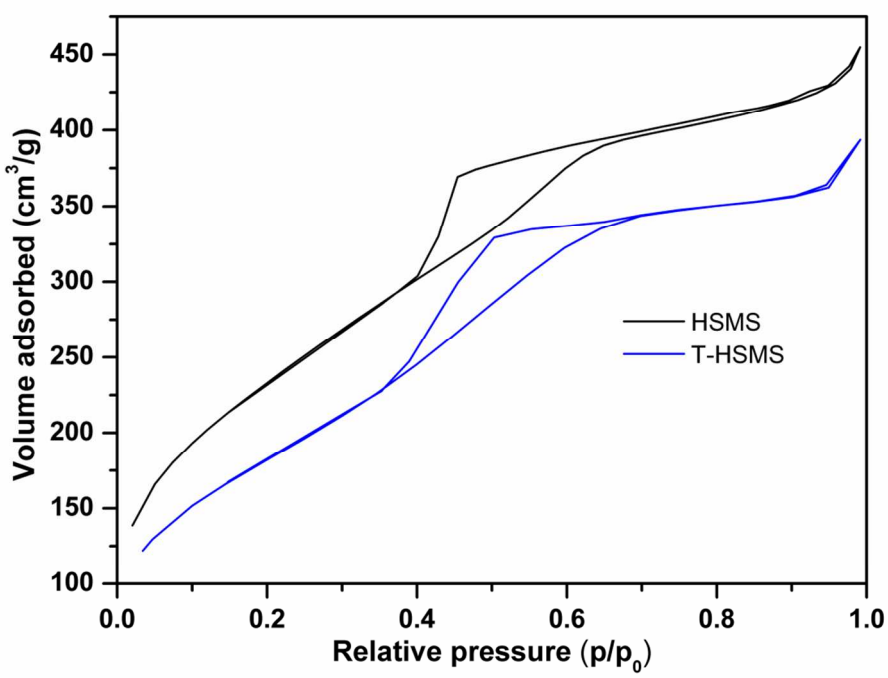

Figure 3: The N_2 adsorption-desorption isotherms of HSMS and T-HSMS.

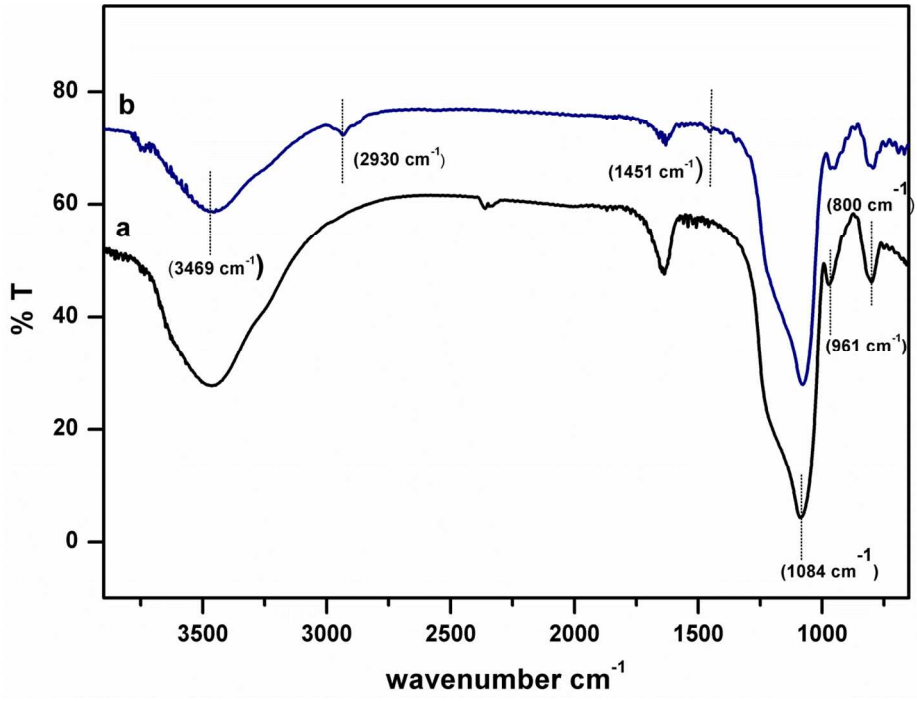

Figure 4: The FT-IR spectra of HSMS (a) and T-HSMS (b).

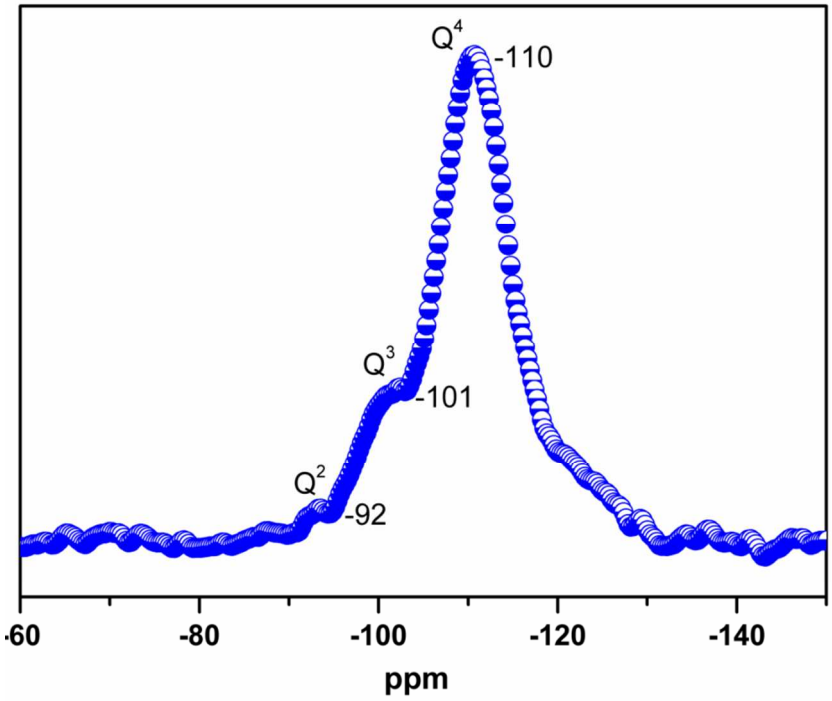

Figure 5: The ^{29}Si CP/MAS NMR spectrum of HSMS

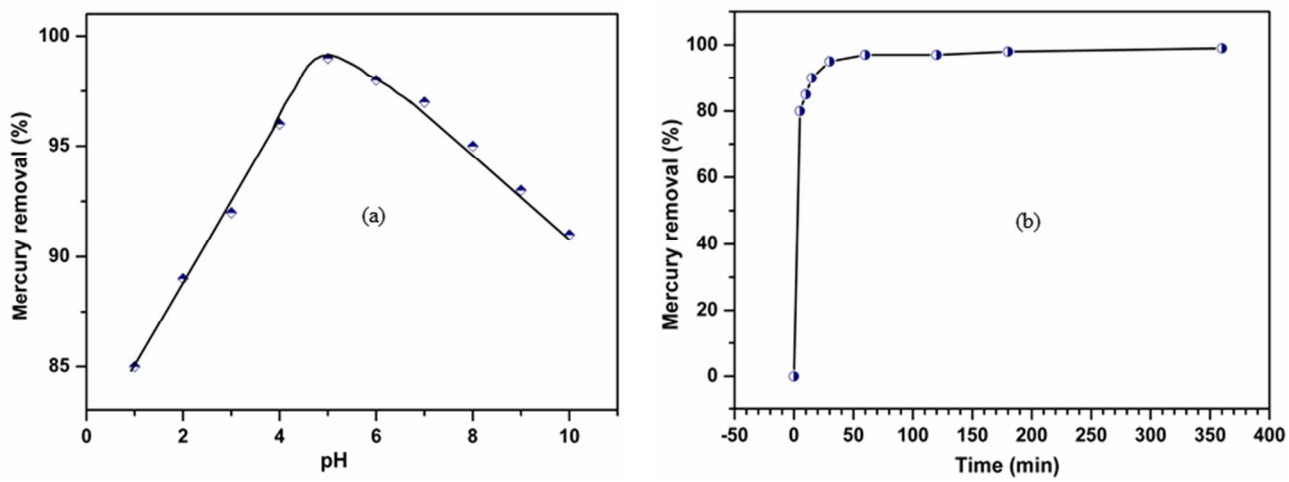

Figure 6: The Mercury removal of T-HSMS a) Effect of pH b) Effect of time

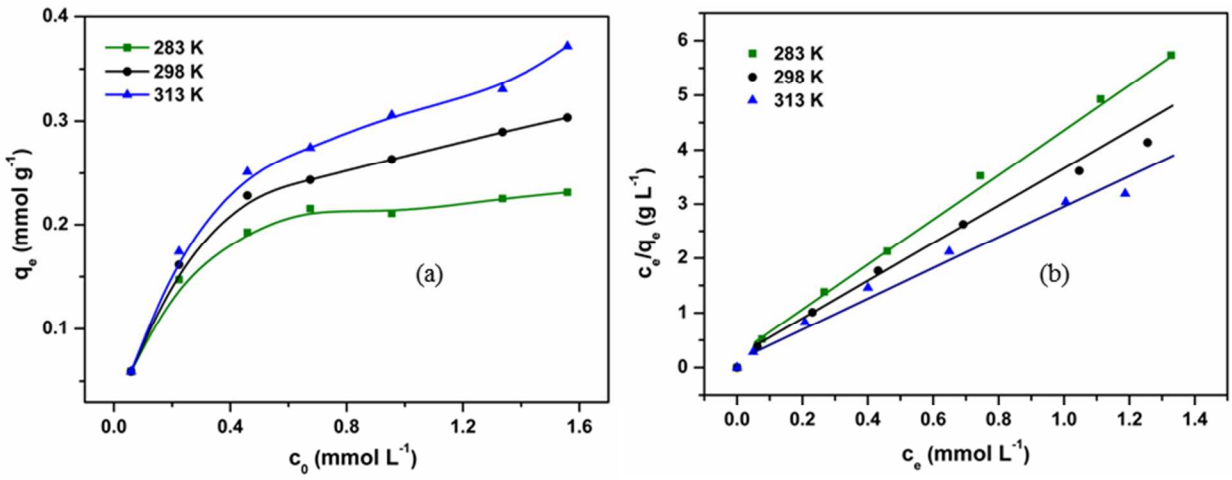

Figure 7: a) The mercury adsorption isotherm of HSMS at three different temperatures, b) the Langmuir adsorption isotherm

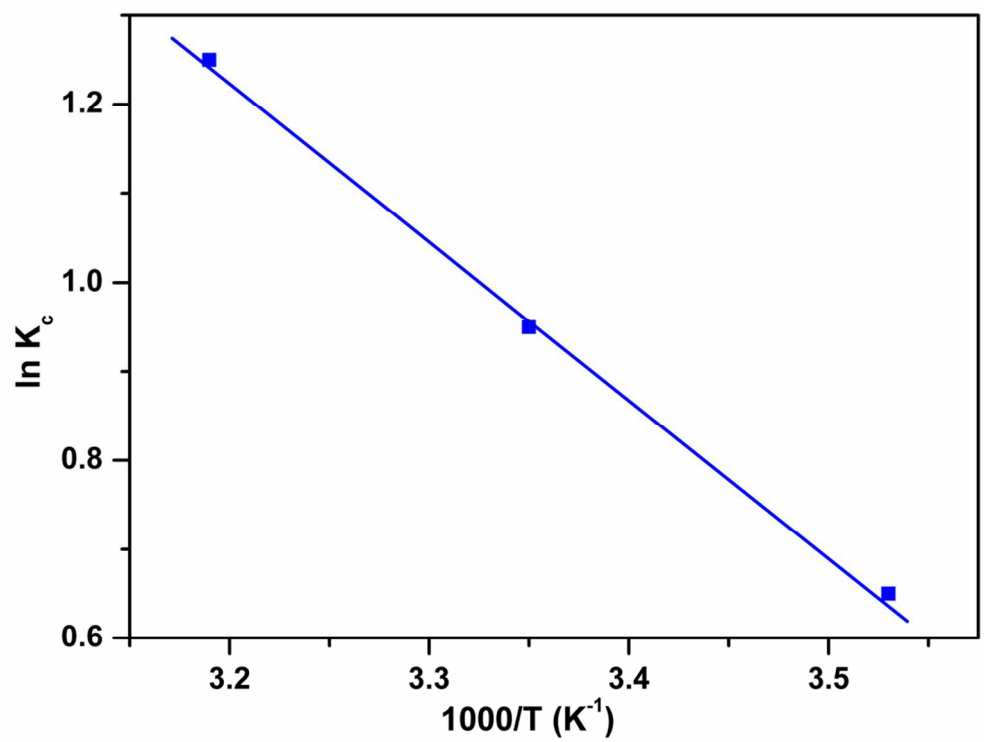

Figure 8: Determination of thermodynamic parameters of mercury adsorption onto T-HSMS

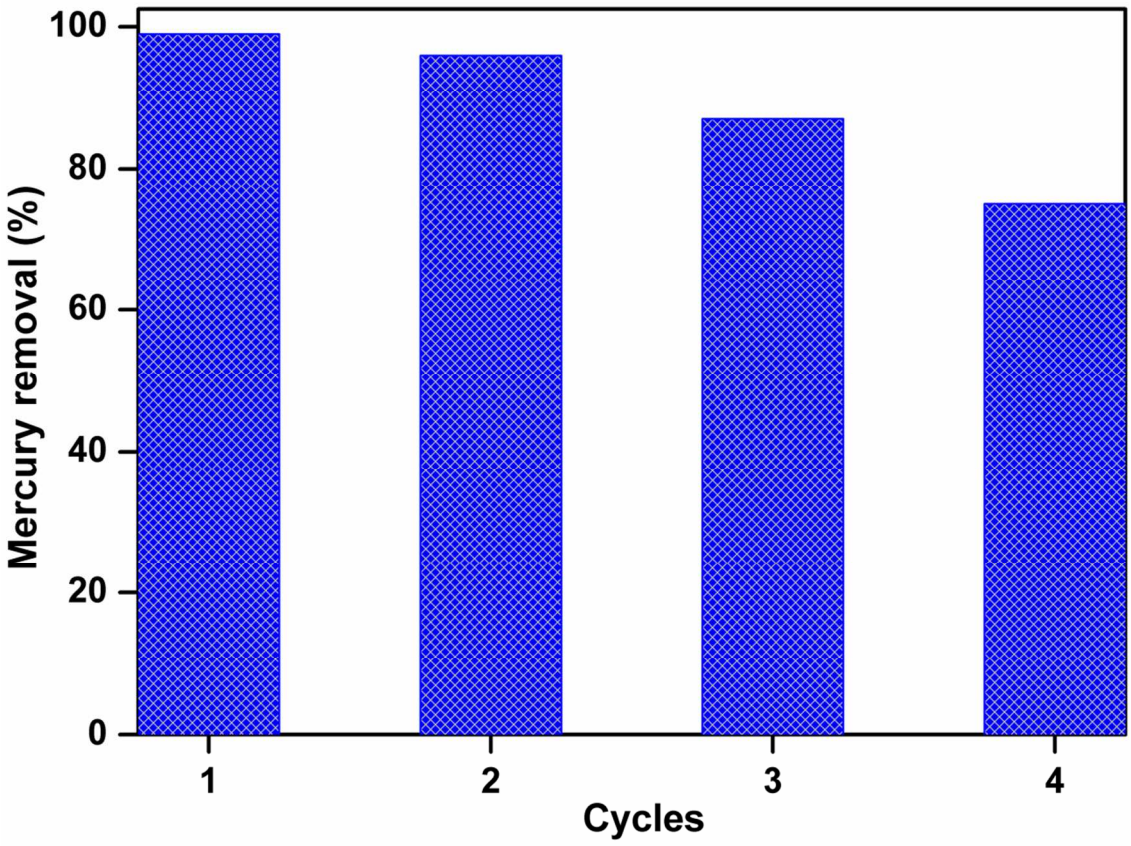

Figure 9: The adsorbent regeneration process.

Tables

Table 1: Textural properties of HSMS and T-HSMS

Materials	d (nm)	S_{BET} (m^2/g)	V_p (cm^3/g)	D_p (nm)	a_0 (nm)	W (nm)	S (mmol/g)
HSMS	10.1	844	0.56	3.2	14.2	11.0	0
T-HSMS	11.3	663	0.27	3.1	15.9	12.8	0.57

d- Inter planar (d_{110}) spacing value, S_{BET}- Surface area, V_p- Pore volume, D_p- Pore diameter, a_0 - unit cell parameter, W- pore wall thickness and S- sulphur content. HSMS-Hierarchically dispersed spherical mesoporous silica, T-HSMS-designated for 3-MPS functionalized HSMS [$d = 2\pi / q$, $a_0 = d_{110}\sqrt{2}$, $W = a_0 - D_p$]

Table 2: Langmuir adsorption isotherm plot values

Temperatures	Langmuir adsorption		
	q_m (mmol/g)	b (L/mmol)	R^2
283 K	0.233	26.18	0.9974
298 K	0.306	15.96	0.9836
313 K	0.367	13.59	0.9830

q_m-maximum adsorption capacity, b-Langmuir constant and R^2-correlation coefficient

Table 3: Mercury adsorption thermodynamics of T-HSMS

ΔH^0 kJ/mol/k	ΔS^0 J/k/mol	ΔG^0 KJ/mol		
		283 K	298 K	313K
14.65	57.03	-1.529	-2.353	-3.252

ΔH^0 - change in enthalpy, ΔS^0 - change in entropy and ΔG^0 - change in Gibbs free energy of mercury adsorption onto T-HSMS.

Graphical abstract

Hierarchically dispersed spherical mesoporous silica (HSMS) was easily synthesized using three surfactants (CTAB, PF127&FC-4), which is successfully modified with thiol groups and used for the mercury adsorption studies.